

Variational calculation of the ppK^- system based on chiral SU(3) dynamics

Akinobu Doté*

High Energy Accelerator Research Organization (IPNS/KEK), 1-1 Oho, Tsukuba, Ibaraki, Japan, 305-0801

Tetsuo Hyodo†

Physik-Department, Technische Universität München, D-85747 Garching, Germany and
Yukawa Institute for Theoretical Physics, Kyoto University, Kyoto 606-8502, Japan

Wolfram Weise‡

Physik-Department, Technische Universität München, D-85747 Garching, Germany

(Dated: September 3, 2018)

The ppK^- system, as a prototype for possible quasibound \bar{K} nuclei, is investigated using a variational approach. Several versions of energy dependent effective $\bar{K}N$ interactions derived from chiral SU(3) dynamics are employed as input, together with a realistic NN potential (Av18). Taking into account theoretical uncertainties in the extrapolations below the $\bar{K}N$ threshold, we find that the antikaonic dibaryon ppK^- is *not* deeply bound. With the driving s -wave $\bar{K}N$ interaction the resulting total binding energy is $B(ppK^-) = 20 \pm 3$ MeV and the mesonic decay width involving $\bar{K}N \rightarrow \pi Y$ is expected to be in the range 40 - 70 MeV. Properties of this quasibound ppK^- system (such as density distributions of nucleons and antikaon) are discussed. The $\Lambda(1405)$, as an $I = 0$ quasi-bound state of \bar{K} and a nucleon, appears to survive in the ppK^- cluster. Estimates are given for the influence of p -wave $\bar{K}N$ interactions and for the width from two-nucleon absorption ($\bar{K}NN \rightarrow YN$) processes. With inclusion of these effects and dispersive corrections from absorption, the ppK^- binding energy is expected to be in the range 20 - 40 MeV, while the total decay width can reach 100 MeV but with large theoretical uncertainties.

PACS numbers: Valid PACS appear here

I. INTRODUCTION

In the context of low-energy QCD with $N_f = 3$ quark flavors, the study of possible antikaon-nuclear quasibound states is a topic of great current interest. Spontaneously broken chiral $SU(3) \times SU(3)$ symmetry, together with explicit symmetry breaking by the non-zero quark masses, basically determines the leading couplings between the low-mass pseudoscalar meson octet (Nambu-Goldstone bosons in the chiral limit) and the octet of the ground state baryons. In particular, the Tomozawa-Weinberg chiral low-energy theorem implies that the driving $\bar{K}N$ interaction in the isospin $I = 0$ channel is strongly attractive. Likewise, the $I = 0$ $\pi\Sigma$ interaction is attractive. The coupling between these $\bar{K}N$ and $\pi\Sigma$ channels is the prime feature governing the subthreshold extrapolation of the $\bar{K}N$ interaction. A detailed knowledge of this subthreshold interaction is required when exploring the possible existence of bound \bar{K} -nuclear clusters.

The quest for strong binding and dropping antikaon masses in a nuclear medium has a long history which originated in early discussions of kaon condensation in dense matter [1, 2] and continued over the years [3–6] with increasing levels of refinement [7]. The topic has

recently been revived when the existence of long-lived, deeply bound \bar{K} -nuclear states was suggested using a simple potential model [8]. It was argued that if the \bar{K} -nuclear binding is sufficiently strong to generate such systems below $\pi\Sigma$ threshold, their width could indeed be small [8, 9]. Experiments performed in search for such states [10–12] have so far not given conclusive answers. While the search continues with more detailed analyses [13–17], “non-exotic” final state interaction scenarios cannot be ruled out as interpretation of the data [18].

An important prototype system for these considerations is ppK^- , the simplest antikaon-nuclear cluster. It has recently been investigated using three-body (Faddeev) methods [19, 20] and variational approaches [21–24]. Reaction studies [25] have also been performed dealing with the actual formation of ppK^- . The Faddeev and variational calculations predict a total ppK^- binding energy in a range $B \sim 50 - 70$ MeV, together with an estimate of the $\bar{K}NN \rightarrow \pi YN$ decay width, $\Gamma \sim 50 - 100$ MeV, depending on details of the interactions used.

The key issue in any such calculation is the (model dependent) extrapolation of the $\bar{K}N$ interaction into the region far below threshold. Its predictive power is so far limited by the persistent lack of accurate constraints from data. It is in this perspective that we perform the present variational calculation using a subthreshold effective $\bar{K}N$ interaction systematically derived from chiral SU(3) coupled-channel dynamics.

Apart from the constraints provided by $\bar{K}N$ threshold data and low-energy cross sections, the only piece

*Electronic address: dote@post.kek.jp

†Electronic address: thyodo@ph.tum.de

‡Electronic address: weise@ph.tum.de

of information about the interaction below $\bar{K}N$ threshold is the $\pi\Sigma$ mass spectrum which is dominated by the $\Lambda(1405)$ resonance. The subthreshold extrapolation of the effective $\bar{K}N$ interaction has recently been investigated in detail [26] from the viewpoint of chiral SU(3) dynamics [27–31]. In this approach the off-shell $\bar{K}N$ amplitude below threshold is governed by the strong attraction in the $\bar{K}N$ and $\pi\Sigma$ channels, and by the dynamical coupling of these channels. These couplings are again determined by the Tomozawa-Weinberg chiral low-energy theorem. Their structure shares features with the early pioneering coupled-channel model [32] that used vector meson exchange interactions (see also Ref. [33]).

Most chiral SU(3) based calculations agree that the $\Lambda(1405)$ resonance structure, with its nominal position at 1405 MeV as seen in the $\pi\Sigma$ mass spectrum, is actually shifted to about 1420 MeV in the $\bar{K}N$ amplitude as a consequence of coupled-channel dynamics. This implies that the effective single-channel $\bar{K}N$ interaction is substantially weaker than anticipated in the simple phenomenological potential used previously in Refs. [8, 21]. In those phenomenological studies, the local, energy-independent potential was adjusted interpreting the $\Lambda(1405)$ directly as a $\bar{K}N$ bound state, identifying its binding energy by the location of the maximum observed in the $\pi\Sigma$ spectrum, but ignoring strong coupled-channel effects.

In this paper we perform a variational ppK^- calculation employing the new effective $\bar{K}N$ potential derived from chiral coupled-channel dynamics [26], together with a realistic NN potential. This calculation is supposed to be complementary to the Faddeev approach with chiral SU(3) constraints [20]. The variational calculation gives easy access to the wave function of the bound state so that valuable information about the structure of the ppK^- cluster can be extracted, whereas the elimination of the $\pi\Sigma$ channel is required and the width of the state can only be estimated perturbatively. The Faddeev calculation has, in turn, the advantage that the decay width of the quasibound state is computed consistently in the coupled-channel framework. Both methods therefore have their virtues and limitations which need to be discussed in comparison.

The present work extends and improves our previous studies [24] in several directions, including further refinements in the NN interaction, computation of density distributions, an evaluation of effects from p -wave $\bar{K}N$ interactions and an estimate of the $\bar{K}NN \rightarrow YN$ absorptive width. The paper is structured as follows. The variational framework and formalism are developed in Sec. II. The derivation of the effective $\bar{K}N$ interaction based on the chiral SU(3) coupled-channel approach is briefly summarized and discussed in Sec. III. Results of our ppK^- calculations are presented in Sec. IV followed by a summary and conclusions in Sec. V.

II. FORMALISM

A. Model wave function

In search for the energetically most favorable $\bar{K}NN$ configuration, the present variational investigation focuses on the ppK^- system with spin and parity $J^\pi = 0^-$ and isospin $(T, T_z) = (1/2, 1/2)$, where the parity assignment includes the intrinsic parity of the antikaon. We prepare the following two-component variational trial wave function:

$$|\Psi\rangle = \mathcal{N}^{-1} [|\Phi_+\rangle + C |\Phi_-\rangle], \quad (1)$$

where \mathcal{N}^{-1} is a normalization factor and C is a mixing coefficient. The components $|\Phi_+\rangle$ and $|\Phi_-\rangle$ have the form

$$|\Phi_+\rangle = \Phi_+(\mathbf{r}_1, \mathbf{r}_2, \mathbf{r}_{\bar{K}}) |S_N = 0\rangle \times \left[[[NN]_{T_N=1} \bar{K}]_{T=1/2, T_z=1/2} \right], \quad (2)$$

$$|\Phi_-\rangle = \Phi_-(\mathbf{r}_1, \mathbf{r}_2, \mathbf{r}_{\bar{K}}) |S_N = 0\rangle \times \left[[[NN]_{T_N=0} \bar{K}]_{T=1/2, T_z=1/2} \right], \quad (3)$$

with spatial wave functions $\Phi_\pm(\mathbf{r}_1, \mathbf{r}_2, \mathbf{r}_{\bar{K}})$ multiplied by the spin state vector of the two nucleons and the isospin state vector of the total $\bar{K}NN$ system, respectively. In both components, the spin of the NN pair is assumed to be zero ($S_N = 0$). The large component $|\Phi_+\rangle$ has isospin ($T_N = 1$) of the two nucleons corresponding to the dominant ppK^- configuration, with inclusion of $pn\bar{K}^0$ through charge exchange. The admixture of the component $|\Phi_-\rangle$ ($T_N = 0$), with zero isospin in the NN sector, can occur through a combination of $I = 0$ and $I = 1$ $\bar{K}N$ interactions and turns out to be small, typically less than 5%. Both components have the same total isospin ($T = 1/2$).

The detailed ansatz for the spatial wave functions is chosen as follows:

$$\begin{aligned} \Phi_\pm(\mathbf{r}_1, \mathbf{r}_2, \mathbf{r}_{\bar{K}}) = & F_N(\mathbf{r}_1) F_N(\mathbf{r}_2) F_K(\mathbf{r}_{\bar{K}}) G(\mathbf{r}_1, \mathbf{r}_2) \\ & \times [H_1(\mathbf{r}_1, \mathbf{r}_{\bar{K}}) H_2(\mathbf{r}_2, \mathbf{r}_{\bar{K}}) \\ & \pm H_2(\mathbf{r}_1, \mathbf{r}_{\bar{K}}) H_1(\mathbf{r}_2, \mathbf{r}_{\bar{K}})] . \quad (4) \end{aligned}$$

Here $F_N(\mathbf{r}_i)$ ($i = 1, 2$) and $F_K(\mathbf{r}_{\bar{K}})$ are trial functions describing the localization of the nucleons and the kaon, respectively. Their forms are assumed to be single Gaussians:

$$F_N(\mathbf{r}_i) = \exp[-\mu \mathbf{r}_i^2], \quad F_K(\mathbf{r}_{\bar{K}}) = \exp[-\gamma \mathbf{r}_{\bar{K}}^2]. \quad (5)$$

The μ and γ in Eq. (5) are treated as independent parameters. Correlations between the two nucleons, and between the \bar{K} and each nucleon, are described by corresponding correlation functions:

$$G(\mathbf{r}_1, \mathbf{r}_2) = 1 - \sum_{n=1}^{N_N} g_n \exp \left[-\lambda_n (\mathbf{r}_1 - \mathbf{r}_2)^2 \right] \quad (6)$$

$$H_a(\mathbf{r}_i, \mathbf{r}_{\bar{K}}) = 1 + \sum_{n=1}^{N_K} h_{a,n} \exp \left[-\nu_n (\mathbf{r}_i - \mathbf{r}_{\bar{K}})^2 \right] \quad (7)$$

The NN correlation function, $G(\mathbf{r}_1, \mathbf{r}_2)$, is prepared to account for the strong short-distance repulsion in the NN interaction which keeps the two nucleons apart. The $\bar{K}N$ correlation functions, $H_a(\mathbf{r}_i, \mathbf{r}_{\bar{K}})$, are given the flexibility to adjust themselves appropriately to the attractive antikaon-nucleon interaction.

One notes that the spatial wave functions $\Phi_{\pm}(\mathbf{r}_1, \mathbf{r}_2, \mathbf{r}_{\bar{K}})$, Eq. (4), are even or odd under exchange of the two nucleons:

$$\Phi_{\pm}(\mathbf{r}_2, \mathbf{r}_1, \mathbf{r}_{\bar{K}}) = \pm \Phi_{\pm}(\mathbf{r}_1, \mathbf{r}_2, \mathbf{r}_{\bar{K}}). \quad (8)$$

The NN pair in $|\Phi_{+}\rangle$ ($|\Phi_{-}\rangle$) is thus in a singlet-even (singlet-odd) state. The spatial wave function is rotationally symmetric, i.e. the total orbital angular momentum is $L = 0$.

The trial wave function has the following real-valued variational parameters: C in Eq.(1), μ and γ in Eq. (5), $\{g_n, \lambda_n\}$ ($n = 1, \dots, N_N$) in Eq. (6), and $\{h_{a,n}, \nu_n\}$ ($n = 1, \dots, N_K$) in Eq. (7). The range parameters of the Gaussians in the NN and $\bar{K}N$ correlation functions are organized as

$$\lambda_n = \lambda_1 \cdot \left(\frac{\lambda_{N_N}}{\lambda_1} \right)^{\frac{n-1}{N_N-1}}, \quad \nu_n = \nu_1 \cdot \left(\frac{\nu_{N_K}}{\nu_1} \right)^{\frac{n-1}{N_K-1}}, \quad (9)$$

independently for each of the NN or $\bar{K}N$ sectors. Various combinations of parameter sets for the Gaussian ranges, μ , γ , $(\lambda_1, \lambda_{N_N})$ and (ν_1, ν_{N_K}) have been tried. For each combination of the range parameters, we find a set of parameters C and $\{g_n; h_{a,n}\}$ which minimizes the expectation value of the total Hamiltonian, using the Simplex method [34]. This determines the $pp\bar{K}^-$ bound state of minimal energy, if existent.

A remark should be added concerning the treatment of the center-of-mass (CM) motion. Given the independence of the variational parameters μ and γ in Eq. (5), the CM wave function cannot simply be separated by factorization in the present model. A complete separation is possible only in the special case $\gamma/\mu = m_K/M_N$, where M_N (m_K) is the nucleon (kaon) mass. In the actual calculations we have confirmed that this relation between γ and μ turns out to be satisfied quite accurately even though it has not been imposed from the beginning. The variational procedure favors indeed a wave function in which the CM motion factorizes as it should. One typically finds $\mu \simeq 0.2 \text{ fm}^{-2}$ and $\gamma \simeq 0.1 \text{ fm}^{-2}$, using the $\bar{K}N$ interaction based on chiral SU(3) dynamics and described in Sec. III.

B. Hamiltonian

The Hamiltonian used in the present study is of the form

$$\hat{H} = \hat{T} + \hat{V}_{NN} + \text{Re} \hat{V}_{\bar{K}N} - \hat{T}_{CM}. \quad (10)$$

Here \hat{T} is the total kinetic energy:

$$\hat{T} = \frac{\hat{\mathbf{p}}_1^2 + \hat{\mathbf{p}}_2^2}{2M_N} + \frac{\hat{\mathbf{p}}_{\bar{K}}^2}{2m_K}. \quad (11)$$

The energy of the center-of-mass motion,

$$\hat{T}_{CM} = \frac{(\hat{\mathbf{p}}_1 + \hat{\mathbf{p}}_2 + \hat{\mathbf{p}}_{\bar{K}})^2}{2(2M_N + m_K)}, \quad (12)$$

is subtracted.

As a realistic nucleon-nucleon interaction \hat{V}_{NN} we choose the Argonne v18 potential (Av18) [35]. Since the total spin of the two nucleons is restricted to zero as explained in the previous section, the tensor, LS and $(LS)^2$ potentials do not contribute. We thus employ the central, L^2 and spin-spin parts of the Av18 potential:

$$\hat{V}_{NN} = \sum_{X=^1E, ^1O} \hat{P}(X) \times \left[v_X^c(r) + v_X^{L^2}(r) \hat{\mathbf{L}}^2 + v_X^{SS}(r) \hat{\boldsymbol{\sigma}}_1 \cdot \hat{\boldsymbol{\sigma}}_2 \right], \quad (13)$$

where $\hat{P}(X)$ is a projection operator onto the singlet-even (1E) or singlet-odd (1O) state, and $\hat{\mathbf{L}}$ is the orbital angular momentum operator for the relative coordinate between two nucleons. The central and L^2 potentials [$v_X^c(r)$ and $v_X^{L^2}(r)$] are identified with the phenomenological short- and intermediate-range parts of the Av18 potential, Eq. (20) in Ref. [35]. The long-range spin-spin term comes from one-pion-exchange, Eq. (17) in Ref. [35]. We ignore the electromagnetic part of Av18. Both 1E and 1O potentials are taken into account since our model wave function includes both types of NN states. In the present study the r -dependence of each of the potential terms is well fitted by a series of Gaussians (see Appendix A). The most pronounced feature is the strong short-distance repulsion in the singlet-even central potential.

The energy-dependent effective s -wave $\bar{K}N$ interaction $\hat{V}_{\bar{K}N}$ is represented as

$$\begin{aligned} \hat{V}_{\bar{K}N} &= \hat{v}(\bar{K}N_1) + \hat{v}(\bar{K}N_2), \quad (14) \\ \hat{v}(\bar{K}N) &= \sum_{I=0,1} \hat{P}_I(\bar{K}N) \\ &\times v_{\bar{K}N}^I(\sqrt{s}) \exp[-(\mathbf{r}_{\bar{K}N}/a_s)^2], \quad (15) \end{aligned}$$

where $\mathbf{r}_{\bar{K}N} = \mathbf{r}_{\bar{K}} - \mathbf{r}_N$ for each of the two nucleons, N_1 and N_2 , and $\hat{P}_I(\bar{K}N)$ is the isospin projection operator for the $\bar{K}N$ pair. In the present work, the radial dependence of the $\bar{K}N$ potential is assumed to be a single Gaussian form with range parameter a_s . The interaction strength $v_{\bar{K}N}^I(\sqrt{s})$ is a function of the (off-shell) center-of-mass energy variable \sqrt{s} of the $\bar{K}N$ system. This interaction, extrapolated into the subthreshold region, is a key issue in the present paper and will be specified in greater detail in a separate Sec. III.

C. Computational procedure

The energy dependence of the $\bar{K}N$ interaction requires a self-consistent variational procedure to minimize the

energy of the $\bar{K}NN$ system. This is done in the same way as in our previous work [22].

We introduce an auxiliary (non-observable) antikaon “binding energy” B_K to control the CM energy \sqrt{s} of the $\bar{K}N$ subsystem within the ppK^- cluster. This B_K is defined as

$$-B_K \equiv \langle \Psi | \hat{H} | \Psi \rangle - \langle \Psi | \hat{H}_N | \Psi \rangle, \quad (16)$$

where \hat{H}_N is the nucleonic part of the Hamiltonian,

$$\hat{H}_N = \hat{T}_N + \hat{V}_{NN} - \hat{T}_{CM,N}, \quad (17)$$

$$\hat{T}_N = \frac{\hat{\boldsymbol{p}}_1^2 + \hat{\boldsymbol{p}}_2^2}{2M_N}, \quad \hat{T}_{CM,N} = \frac{(\hat{\boldsymbol{p}}_1 + \hat{\boldsymbol{p}}_2)^2}{4M_N}. \quad (18)$$

The relation between the $\bar{K}N$ two-body energy \sqrt{s} and B_K within the three-body system is not *a priori* fixed. In general,

$$\sqrt{s} = M_N + m_K - \eta B_K, \quad (19)$$

where η is a parameter describing the balance of the antikaon energy between the two nucleons of the $\bar{K}NN$ three-body system. One expects $1/2 \leq \eta \leq 1$. The upper limit ($\eta = 1$) corresponds to the case in which the antikaon field collectively surrounds the two nucleons, a situation encountered in the limit of static (infinitely heavy) nucleon sources. In the lower limit ($\eta = 1/2$) the antikaon energy is split symmetrically half-and-half between the two nucleons. We investigate both cases and label them “Type I” and “Type II”, respectively:

$$\text{Type I :} \quad \sqrt{s} = M_N + m_K - B_K, \quad (20)$$

$$\text{Type II :} \quad \sqrt{s} = M_N + m_K - B_K/2. \quad (21)$$

The calculations then proceed as follows. First, assume B_K to be some trial starting value, $B_K^{(0)}$. Given a relation between B_K and \sqrt{s} , the strength of the $\bar{K}N$ potential is now fixed, and the Hamiltonian is determined. Then the variational calculation is performed to find the state of minimal energy. Given that state, a new antikaon binding energy, $B_K^{(1)}$, is evaluated with the wave function so obtained. Then one examines whether $B_K^{(1)}$ coincides with $B_K^{(0)}$. If not, a different starting value $B_K^{(0)}$ is chosen and the procedure is repeated until $B_K^{(1)} = B_K^{(0)}$ is satisfied at an acceptable level of accuracy.

The $\bar{K}N$ potential is in general complex. In order to perform the variational calculation of the energy and the “bound state” $|\Psi\rangle$, the real part of the potential, $\text{Re } \hat{V}_{\bar{K}N}$, is used as a starting point. The decay width Γ of that state is then calculated perturbatively by taking the expectation value of the imaginary part of the $\bar{K}N$ potential:

$$\Gamma = -2 \langle \Psi | \text{Im } \hat{V}_{\bar{K}N} | \Psi \rangle. \quad (22)$$

At this stage the width Γ represents the mesonic two-body decay channels ($\bar{K}N \rightarrow \pi\Sigma, \pi\Lambda$) within the $\bar{K}NN$ three-body system. The non-mesonic absorption width for $\bar{K}NN \rightarrow \Sigma N, \Lambda N$ will be treated separately.

III. EFFECTIVE $\bar{K}N$ INTERACTION

A. $\bar{K}N$ potential based on chiral SU(3) dynamics

Here we discuss the effective $\bar{K}N$ potential developed in Ref. [26]. This potential has been systematically constructed using chiral SU(3) coupled-channel calculations which successfully describe $S = -1$ meson-baryon scattering and the properties of the dynamically generated $\Lambda(1405)$ resonance. The formulation of the coupled-channel approach is briefly sketched in Appendix B. Starting from this coupled-channel framework, a complex and energy-dependent interaction kernel V^{eff} is derived in the single $\bar{K}N$ channel, such that the full coupled-channel s -wave $\bar{K}N$ scattering amplitude is exactly reproduced by solving the single-channel equation with V^{eff} . Then this effective interaction kernel is approximated by an equivalent local $\bar{K}N$ potential used in the Schrödinger equation (with reduced $\bar{K}N$ mass μ),

$$-\frac{d^2 u(r)}{dr^2} + 2\mu [U(r, \sqrt{s}) + B] u(r) = 0. \quad (23)$$

The potential $U(r, \sqrt{s})$ is expressed by the effective interaction kernel $V^{\text{eff}}(\sqrt{s})$ together with a normalized spatial distribution $g(r)$,

$$U(r, \sqrt{s}) = \frac{g(r)}{2\tilde{\omega}} \frac{M_N}{\sqrt{s}} V^{\text{eff}}(\sqrt{s}), \quad (24)$$

where r is the relative coordinate of the $\bar{K}N$ system and $\tilde{\omega} = [s^2 - (M_N^2 - m_K^2)^2]/(4s^{3/2})$ is the reduced energy of the $\bar{K}N$ two-body system.

An important observation in Ref. [26] and earlier work is that the $\pi\Sigma$ diagonal coupling is strong enough to generate a resonance in the single (elastic) $\pi\Sigma$ channel. In the strongly interacting $\bar{K}N \leftrightarrow \pi\Sigma$ system, the $\Lambda(1405)$ appears as a $\bar{K}N$ bound state embedded in the resonant $\pi\Sigma$ continuum. The experimentally observed broad spectrum in the $\pi\Sigma$ channel, with its maximum at 1405 MeV, is dominated by the inherent $\pi\Sigma$ interaction, while the resonant structure in the $\bar{K}N$ amplitude, governed by the inherent $\bar{K}N$ interaction, actually appears around 1420 MeV. The $\bar{K}N$ “binding energy” commonly associated with the $\Lambda(1405)$ is therefore not 27 MeV but only less than half of this naive estimate. This small $\bar{K}N$ binding energy implies a weaker attractive potential, only about half as strong as the phenomenological potential of Refs. [8, 21]. One should nonetheless note that both phenomenological and chiral potentials reproduce the existing experimental data around threshold. Their qualitatively different subthreshold extrapolations result from the fact that the coupled-channels framework, constrained by the chiral effective Lagrangian, induces off-shell dynamics which is very different from the purely phenomenological approach.

Here we choose the spatial distribution of the potential as a Gaussian form

$$U(r, \sqrt{s}) = v_{\bar{K}N}^I(\sqrt{s}) \exp[-(r/a_s)^2], \quad (25)$$

where a_s is the range parameter. The strength of the approximate local potential is related to the interaction kernel $V^{\text{eff}}(\sqrt{s})$ defined in Ref. [26] as

$$v_{\bar{K}N}^I(\sqrt{s}) = \frac{M_N}{2\pi^{3/2} a_s^3 \tilde{\omega} \sqrt{s}} V^{\text{eff}}(\sqrt{s}). \quad (26)$$

The potential so obtained is complex and energy dependent, reflecting the elimination of the other (mainly $\pi\Sigma$) channels. The center-of-mass energy \sqrt{s} is related to the binding energy B of the $\bar{K}N$ two-body system B as

$$B = -\sqrt{s} + M_N + m_K.$$

We choose the range parameter a_s such that the resonance structure is reproduced at the position predicted by the full chiral dynamics calculation. The scattering amplitudes for both $I = 0$ and $I = 1$ around $\bar{K}N$ threshold are also well reproduced by this potential.

However, the effective single-channel $\bar{K}N$ effective interaction V^{eff} is generally *non-local*. Naive translation of V^{eff} into an approximate *local* form does not guarantee that this local potential (we refer to it as “uncorrected”) reproduces the $\bar{K}N$ amplitude of the full coupled-channel calculation over a wide range of subthreshold energies. It is indeed found that simple extrapolation of the local potential (26) to the deep subthreshold region, $\sqrt{s} < 1400$ MeV, significantly overestimates the scattering amplitude in comparison with that of the original coupled-channel approach [26]. Compensation of this deficiency requires modifying the strength of the real part of the potential and introducing extra energy dependence. The strengths of these “corrected” potentials in the $I = 0$ and $I = 1$ channels are parametrized by polynomials as

$$v_{\bar{K}N}^I(\sqrt{s}) = K_{I,0} + K_{I,1} s^{1/2} + K_{I,2} s + K_{I,3} s^{3/2}. \quad (27)$$

The coefficients $K_{I,i}$ are given in Ref. [26]. The strengths of the “corrected” and “uncorrected” potentials at $r = 0$ are shown in Fig. 1, based on the chiral model of Ref. [37]. For the subsequent variational three-body calculation we always use the “corrected” potentials.

In order to estimate theoretical uncertainties we use altogether four different variants of chiral dynamics calculations from which we derive equivalent energy-dependent local potentials, ORB [36], HNJJ [37], BNW [38], and BMN [39]. All these models reproduce the total cross sections for elastic and inelastic K^-p scattering, threshold branching ratios, and the $\pi\Sigma$ mass spectrum associated with the $\Lambda(1405)$. Differences among those models mainly stem from the lack of accurate data for the $\pi\Sigma$ spectrum and from differences in details of the fitting procedures. The values of the range parameters for these models are shown in the second row in Table I. Additional uncertainties, concerning higher order terms in the interaction kernel derived from chiral SU(3) dynamics, are estimated to be about 20 % around $\sqrt{s} \sim 1360$ MeV, based on the systematic study of such higher order corrections in Ref. [38].

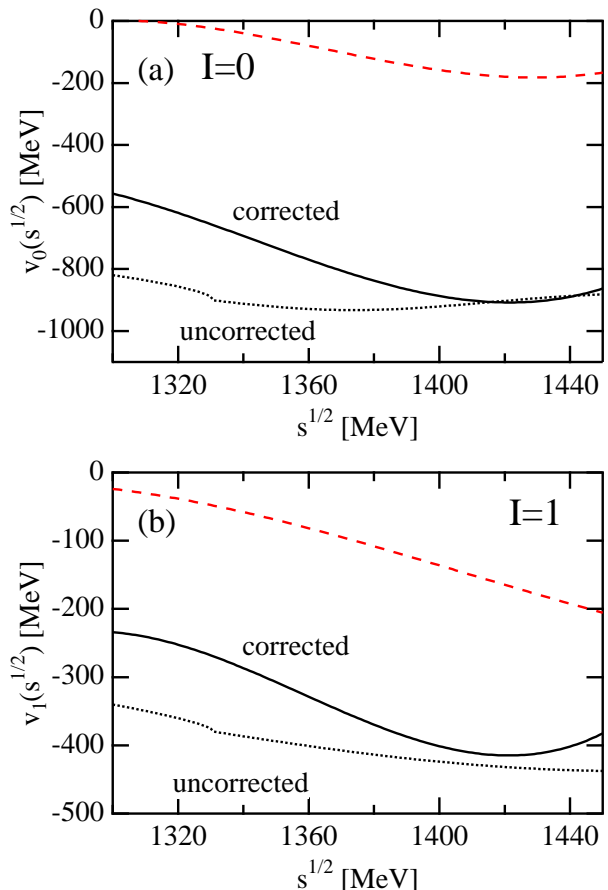


FIG. 1: (Color online) Strength of the “corrected” (solid lines) and “uncorrected” (dotted lines) potentials at $r = 0$ with HNJJ model [37]. The real parts are shown as solid/dotted lines. Imaginary parts are given as dashed lines. (a): $I = 0$ channel, (b): $I = 1$ channel.

B. Structure of the $\Lambda(1405)$

Let us now examine the two-body $\bar{K}N$ system with $I = 0$ where the $\Lambda(1405)$ is generated dynamically below the $\bar{K}N$ threshold. In order to study the structure of the $\Lambda(1405)$, we first solve the Schrödinger equation (23) with the real part of the potential, $\text{Re}[U(r, \sqrt{s})]$. This treatment appears to be justified by the relatively small imaginary part of the potential as seen in Fig. 1. Corrections from the dispersive shift of the binding energy induced by the imaginary part of the potential will be estimated as we move along.

The self-consistent results for the binding energies are summarized in Table I together with the root mean distance ($\sqrt{\langle r^2 \rangle}$) between antikaon and nucleon which form the $\Lambda(1405)$. These results are produced with the “corrected” potentials, but the “uncorrected” ones give essentially the same output since the difference in strength between the “corrected” and “uncorrected” potentials is small in the energy region relevant to the $\bar{K}N$ bound

TABLE I: Range parameters a_s of the local $\bar{K}N$ potential, the self-consistent $\bar{K}N$ binding energy B , and the root mean distance $\sqrt{\langle r^2 \rangle}$ between antikaon and nucleon. The energies B_1 and B_2 are determined, respectively, by the zero of the real part and the maximum of the imaginary part of the full amplitude with complex potential (see text).

	ORB [36]	HNJH [37]	BNW [38]	BMN [39]
a_s [fm]	0.52	0.47	0.51	0.41
B [MeV]	11.8	11.5	9.97	13.3
$\sqrt{\langle r^2 \rangle}$ [fm]	1.87	1.86	1.99	1.72
B_1 [MeV]	16.5	15.5	17.0	16.7
B_2 [MeV]	17.8	16.9	19.8	18.9

state ($\sqrt{s} \sim 1420$ MeV). The typical $\bar{K}N$ binding energy and root mean distance found with the chiral potential,

$$B \sim 12 \text{ MeV}, \quad \sqrt{\langle r^2 \rangle} \sim 1.9 \text{ fm}, \quad (28)$$

should be compared with the results of the phenomenological model [21]: $B = 27$ MeV and $\sqrt{\langle r^2 \rangle} = 1.36$ fm. The small binding obtained with the present potential is related to the strong $\pi\Sigma$ interaction in chiral dynamics, as discussed in Ref. [26]. Since the binding energy is smaller, the size of the bound state becomes correspondingly larger than that of the phenomenological model.

It is instructive to recall the study of electromagnetic properties of the $\Lambda(1405)$ in chiral dynamics [40], where a relatively large electric mean squared radius has been reported. Although the electric mean squared radius is not directly comparable to the mean distance of antikaon and nucleon, qualitative agreement of these independent size estimates gives support to the chiral effective potential introduced here, while the radius in Ref. [40] was computed with the full chiral coupled-channel amplitudes.

C. Dispersive effects induced by the imaginary part of the potential

The variational calculation of the ppK^- three-body problem has the disadvantage (unlike the Faddeev approach) that only the real part of the complex $\bar{K}N$ potential can be handled as input whereas the imaginary part must be treated perturbatively. It is therefore mandatory to estimate the systematic uncertainties caused by this limitation.

In the $\bar{K}N$ two-body case, the scattering amplitude can easily be obtained by solving Eq. (23) with the full complex potential. Effects of the dispersive shift on the binding energy, induced by the imaginary part of this potential, can then be examined by comparing the full result (with complex potential) to the one obtained using only the real part of the potential, see Eq.(28). The

energy, B_1 , of the subthreshold $\bar{K}N$ state generated by the complex potential can be deduced from the zero of the real part of the $\bar{K}N$ scattering amplitude. For comparison we also check the position of the maximum, B_2 , of the imaginary part of that amplitude, which coincides with B_1 if the non-resonant background is small.

The calculated values of B_1 (and B_2) are listed, for all models considered, in Table I. Comparing B_1 with the binding energies B found with the real parts of the potentials, we conclude that the dispersive effects may increase the binding energy of the $\bar{K}N$ two-body quasi-bound state by

$$\Delta B \sim 3 - 7 \text{ MeV}, \quad (29)$$

or $\Delta B \sim 6 - 10$ MeV when comparing B_2 and B . We keep this shift ΔB in mind for a discussion of systematic uncertainties when we now turn to the $\bar{K}NN$ three-body system.

IV. RESULTS

This section presents the results of our variational calculations of the quasibound ppK^- system. Four variants of effective $\bar{K}N$ interactions have been employed: ORB, HNJH, BNW and BMN as explained in the previous section. These interactions are translated into local, energy-dependent potentials. In all cases we have used the ‘‘corrected’’ versions of the potentials which properly reproduce the $\bar{K}N$ scattering amplitude computed with full chiral coupled-channel dynamics. In the self-consistent treatment of the energy dependence of the interaction, both options, ‘‘Type I’’ [Eq. (20)] and ‘‘Type II’’ [Eq. (21)] for the relationship between \sqrt{s} and B_K have been tried. With these different choices for on-shell equivalent potentials and different options for handling off-shell energies within the three-body system, we are in a position to give rough estimates of the uncertainties associated with the required subthreshold extrapolations. In all calculations, the convergence of the Gaussian expansions (6) and (7) has been checked and found satisfactory with $N_N = N_K = 5$.

A. Total binding energy and decay width

The results of self-consistent solutions for total ppK^- binding energies are summarized together with the $\bar{K}NN \rightarrow \pi YN$ decay widths in Table II and depicted in Fig. 2. In all present calculations the binding energies turn out to be quite modest. Deeply bound, narrow ppK^- states are not seen to develop. The variational calculations, with $\text{Re}V_{\bar{K}N}$ as previously specified and $\text{Im}V_{\bar{K}N}$ treated according to Eq.(22), predicts total binding energies and decay widths in the range

$$B(ppK^-) \sim 20 \pm 3 \text{ MeV} \quad \text{and} \quad \Gamma \sim 40 - 70 \text{ MeV}$$

TABLE II: Results of variational calculations for ppK^- binding energies and $(\bar{K}NN \rightarrow \pi YN)$ decay widths Γ based on four versions of chiral effective $\bar{K}N$ potentials. “ORB” etc. indicate the chiral SU(3) model used in each case. The “corrected” equivalent local potentials have been adopted throughout, with ranges a_s given in Table I. “Type I (II)” refers to the ansatz for the relationship between \sqrt{s} and B_K (see text).

	ORB	HNJH	BNW	BMN
“Type I”				
$B(ppK^-)$ [MeV]	18.9	16.9	18.1	16.6
Γ [MeV]	53.1	47.0	60.4	38.8
“Type II”				
$B(ppK^-)$ [MeV]	22.7	20.8	20.7	21.7
Γ [MeV]	64.2	58.3	71.4	53.1

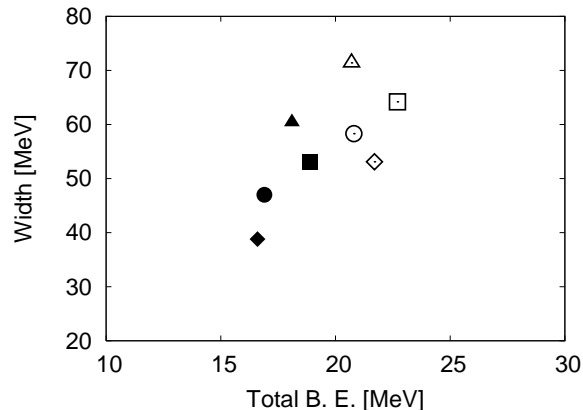


FIG. 2: Distribution of total binding energy and mesonic decay width. The models “ORB”, “HNJH”, “BNW” and “BMN” are shown with symbols square, circle, triangle and diamond, respectively. Closed (Open) symbols indicate the “Type I” (“Type II”) ansatz.

for all cases studied. The “Type II” ansatz favors slightly stronger binding (20 - 23 MeV) than the “Type I” option (16 - 19 MeV). Different potentials produce binding energy variations within only about two MeV for each given “Type I” or “Type II” set.

It is instructive to examine the detailed decomposition of the total ppK^- energy into kinetic and potential energies of the antikaon and two-nucleon subcomponents. These sets of numbers are given in Tables III and IV for the four variants of chiral SU(3) based models mentioned previously. Shown (separately for the “Type I” and “Type II” options) are the total kinetic energy, $E_{kin} = \langle \Psi | \hat{T} - \hat{T}_{CM} | \Psi \rangle$, the nuclear part of the kinetic energy, $T_{nuc} = \langle \Psi | \hat{T}_N - \hat{T}_{CM,N} | \Psi \rangle$, the antikaon binding energy B_K defined in Eq. (16), the expectation value of the \bar{K} -nuclear potential energy, $V(\bar{K}N) = \langle \Psi | \text{Re } \hat{V}_{\bar{K}N} | \Psi \rangle$,

and the contribution from the nucleon-nucleon interaction, $V(NN) = \langle \Psi | \hat{V}_{NN} | \Psi \rangle$.

Several interesting observations can be made. First, the kaon “binding energy” B_K is in the range 40 - 50 MeV for all cases studied. Note, however, once again that B_K is *not* an observable in the $\bar{K}NN$ three-body system. In fact the observable total ppK^- binding energy is less than half of B_K . The nucleons are the slow movers in the quasibound compound: their kinetic energies add up to only about 40 MeV, while the total kinetic energy in the three-body cluster is typically more than three times larger and thus carried predominantly by the antikaon floating between the two slowly moving, heavy nucleons. The antikaon’s potential energy roughly cancels the total kinetic energy, leaving room for the nucleon-nucleon interaction to bind the system which, as an isolated proton-proton pair, would be unbound.

The admixture of the isospin-zero ($T_N = 0$) component $|\Phi_-\rangle$ [Eq. (3)] is typically about 4%. It originates from the coupling matrix element $\langle \Phi_+ | \hat{V}_{\bar{K}N} | \Phi_-\rangle$ which is proportional to the difference of $I = 0$ and $I = 1$ $\bar{K}N$ interactions. Although small, this admixture helps binding the ppK^- system: without the $|\Phi_-\rangle$ component, the total binding energy would decrease by about 5 - 7 MeV as seen from the lines denoted “HNJH † ” in Tables III and IV.

The spin-spin and L^2 parts of the NN potential have an influence on the $|\Phi_-\rangle$ admixture. The contribution of these terms to $V(NN)$ is small and attractive. It tends to reduce the mixing of the $|\Phi_-\rangle$ component into the total wave function. This is seen in the last lines of Tables III and IV denoted by “HNJH*” where the spin-spin and L^2 potentials are turned off and only the central part of the NN potential is active. The spin-spin and L^2 terms were not considered in our previous Ref. [24].

B. Structure of the ppK^- cluster

Consider now the more detailed structure and characteristic sizes of the ppK^- system as found in the present calculations. For this purpose we introduce density distributions of the NN and $\bar{K}N$ pairs in the quasibound compound as functions of the respective nucleon-nucleon and antikaon-nucleon distances, as follows:

$$\rho_{NN}(\mathbf{x}) = \langle \Psi | \delta^3(\mathbf{r}_1 - \mathbf{r}_2 - \mathbf{x}) | \Psi \rangle, \quad (30)$$

$$\rho_{\bar{K}N}(\mathbf{x}) = \langle \Psi | \frac{1}{2} \sum_{i=1,2} \delta^3(\mathbf{r}_{\bar{K}} - \mathbf{r}_i - \mathbf{x}) | \Psi \rangle, \quad (31)$$

where $\mathbf{r}_{1,2}$ refer to the two nucleons and $\mathbf{r}_{\bar{K}}$ to the antikaon. Both densities are understood as being normalized to one. The projected density distributions for $\bar{K}N$ pairs with specific isospin $I = 0, 1$ are

$$\rho_{\bar{K}N}^I(\mathbf{x}) = \langle \Psi | \frac{1}{2} \sum_{i=1,2} \hat{P}_I(\bar{K}N_i) \delta^3(\mathbf{r}_{\bar{K}} - \mathbf{r}_i - \mathbf{x}) | \Psi \rangle. \quad (32)$$

TABLE III: Detailed compilation of ppK^- results calculated for chiral SU(3) models ORB, HNJV, BNW and BMN (see text) with the ‘‘Type I’’ ansatz for the relation between antikaon binding energy B_K and \sqrt{s} in the off-shell $\bar{K}N$ two-body subsystem. The listing includes: the total binding energy $B(ppK^-)$ and decay width Γ for $\bar{K}NN \rightarrow \pi YN$; the total kinetic energy, $E_{kin} = \langle \Psi | \hat{T} - \hat{T}_{CM} | \Psi \rangle$, the nuclear part of the kinetic energy, $T_{nuc} = \langle \Psi | \hat{T}_N - \hat{T}_{CM,N} | \Psi \rangle$; the antikaon binding energy B_K as defined in Eq.(16); the \bar{K} -nuclear potential energy, $V(\bar{K}N) = \langle \Psi | \text{Re} \hat{V}_{\bar{K}N} | \Psi \rangle$; the contribution from the nucleon-nucleon interaction, $V(NN) = \langle \Psi | \hat{V}_{NN} | \Psi \rangle$, with all entries given in MeV. Lower part of table: percentage $P(T_N = 0)$ of the $|\Phi_- \rangle$ admixture to the total wave function; r.m.s. distances R_{NN} and $R_{\bar{K}N}$ between the two nucleons, and between antikaon and a nucleon; r.m.s. distances between antikaon and nucleon, $R_{\bar{K}N} (I = 0, 1)$, for isospins $I = 0, 1$ of the $\bar{K}N$ pair (all given in fm). Lines denoted HNJV[†] are calculated switching off the admixture of the $|\Phi_- \rangle$ component. Lines HNJV* are results obtained without the spin-spin and L^2 potentials of the NN potential. (Both these cases refer to the $\bar{K}N$ potential derived from the HNJV model).

	$B(ppK^-)$	Γ	E_{kin}	T_{nuc}	B_K	$V(\bar{K}N)$	$V(NN)$
ORB	18.9	53.1	125.9	38.3	40.2	-127.7	-17.0
HNJV	16.9	47.0	129.5	38.1	38.9	-130.4	-16.2
BNW	18.1	60.4	124.9	37.4	39.2	-126.7	-16.3
BMN	16.6	38.8	141.5	39.9	40.8	-142.5	-15.7
HNJV [†]	12.0	44.8	115.1	37.0	31.0	-109.0	-18.2
HNJV*	15.9	47.1	129.6	37.3	38.9	-131.2	-14.3

	$P(T_N = 0)$	R_{NN}	$R_{\bar{K}N}$	$R_{\bar{K}N} (I = 0)$	$R_{\bar{K}N} (I = 1)$
ORB	3.4 %	2.15	1.93	1.79	2.28
HNJV	3.8 %	2.21	1.97	1.82	2.33
BNW	4.1 %	2.20	1.97	1.81	2.35
BMN	3.8 %	2.23	2.00	1.86	2.34
HNJV [†]	0 %	2.13	2.01	2.01	2.01
HNJV*	4.5 %	2.26	2.00	1.83	2.39

TABLE IV: Same as Table III, but using the ‘‘Type II’’ ansatz for the relation between antikaon binding energy B_K and \sqrt{s} in the off-shell $\bar{K}N$ two-body subsystem.

	$B(ppK^-)$	Γ	E_{kin}	T_{nuc}	B_K	$V(\bar{K}N)$	$V(NN)$
ORB	22.7	64.2	136.0	40.9	46.1	-141.2	-17.6
HNJV	20.8	58.3	141.0	40.9	45.1	-145.2	-16.6
BNW	18.1	71.4	132.0	39.3	43.2	-136.0	-16.7
BMN	21.7	53.1	158.4	43.8	49.3	-163.9	-16.2
HNJV [†]	13.8	51.8	121.3	38.7	33.9	-116.5	-18.5
HNJV*	19.8	58.6	141.5	40.3	45.2	-146.4	-14.9

	$P(T_N = 0)$	R_{NN}	$R_{\bar{K}N}$	$R_{\bar{K}N} (I = 0)$	$R_{\bar{K}N} (I = 1)$
ORB	3.7 %	2.10	1.85	1.71	2.21
HNJV	4.1 %	2.15	1.89	1.73	2.26
BNW	4.1 %	2.16	1.91	1.75	2.29
BMN	4.1 %	2.15	1.89	1.73	2.25
HNJV [†]	0 %	2.09	1.96	1.96	1.96
HNJV*	4.8 %	2.19	1.91	1.74	2.31

with the isospin projectors $\hat{P}_I(\bar{K}N_i)$.

With these distributions one can determine mean-square distances

$$R_{NN}^2 = \int d^3\mathbf{x} \mathbf{x}^2 \rho_{NN}(\mathbf{x}), \quad (33)$$

$$R_{\bar{K}N}^2 = \int d^3\mathbf{x} \mathbf{x}^2 \rho_{\bar{K}N}(\mathbf{x}), \quad (34)$$

$$R_{\bar{K}N}^2(I) = N_I^{-1} \int d^3\mathbf{x} \mathbf{x}^2 \rho_{\bar{K}N}^I(\mathbf{x}), \quad (35)$$

with $N_I = \int d^3\mathbf{x} \rho_{\bar{K}N}^I(\mathbf{x})$. These average distances are summarized in the lower parts of Tables III and IV. The relatively weak binding of the system implies rather large NN distances, typically around $R_{NN} \simeq 2.2$ fm, while the average $\bar{K}N$ distances are slightly smaller, $R_{\bar{K}N} \simeq 1.9-2$ fm. When looked at separately in the $I = 0$ and $I = 1$ channels of the $\bar{K}N$ subsystem, the significantly stronger attraction in the $I = 0$ component drags the antikaon closer to the nucleon than in the $I = 1$ component.

The different density distributions, Eqs. (30-32), are

shown in Figs. 3 and 4. These densities depend only on the absolute value of the relative coordinate \boldsymbol{x} . The two-body densities are plotted as functions of $r = |\boldsymbol{x}|$ and normalized as $4\pi \int dr r^2 \rho(r) = 1$. The two-nucleon distribution ρ_{NN} shows the pronounced effect of the short-distance repulsive core of the NN interaction. The maximum NN density reached in this weakly bound system is about 0.03 fm^{-3} , a small fraction of typical bulk nuclear densities and only twice as large as the maximum proton-neutron density in the even more dilute, very weakly bound deuteron.

The $\bar{K}N$ density distribution has its maximum at zero distance between the antikaon and each nucleon. It reflects the strong $\bar{K}N$ attraction in the $I = 0$ channel, whereas the $I = 1$ $\bar{K}N$ density is small. The right panel in Fig. 4 shows a comparison between densities of the $I = 0$ $\bar{K}N$ pair in the ppK^- cluster and the one forming the $\Lambda(1405)$ as a two-body $\bar{K}N$ quasibound state. Both densities are properly normalized for the comparison. The conclusion to be drawn from this picture is that the $\Lambda(1405)$ stays essentially intact in the ppK^- system which appears to behave much like a weakly bound, short-lived $p\Lambda(1405)$ compound. Again, the $I = 1$ component of the total $\bar{K}N$ density is small. A detailed analysis of the expectation values of the squared angular momentum, $L_{\bar{K}N}^2$ in the ppK^- system shows that it is close to zero in $I = 0$ and close to two in $I = 1$ $\bar{K}N$ configurations, indicating as expected the dominant s -wave in the $I = 0$ channel. The survival of the $\Lambda(1405)$ in the three-body cluster is qualitatively consistent with the result of the phenomenological potential [21].

C. Comparison with Faddeev results

The small ppK^- binding energy of only about 20 MeV found in the present variational approach appears to be inconsistent with results of a Faddeev calculation using a chiral interaction [20] which predicts about 80 MeV binding. Here we discuss possible reasons for this difference.

An advantage of the Faddeev treatment is its capability to treat the three-body dynamics in the $\pi\Sigma N$ channel. The variational approach, on the other hand, works with an effective $\bar{K}N$ interaction after eliminating the $\pi\Sigma$ channel. While the attractive $\pi\Sigma$ two-body interactions and their coupled-channel effects are nonetheless accounted for as part of the complex and energy dependent $\bar{K}N$ potential, additional attraction may indeed be generated by the $\pi\Sigma N$ three-body dynamics treated explicitly in the Faddeev approach.

Secondly, there are significant differences in the subthreshold extrapolations of the two-body $\bar{K}N$ interaction. When solving Faddeev equations, a one-term separable form has been used to approximate the $\bar{K}N$ interaction [20]. While this interaction agrees with ours in its on-shell properties around $\bar{K}N$ threshold, it has been pointed out in Ref. [26] that using such a separable approximation gives stronger attraction at lower

(subthreshold) energies, as an artifact of the regularization procedure. This is also evident by comparison of subthreshold extrapolations with early works on chiral $SU(3)$ coupled-channel dynamics which had adopted separable forms for the $\bar{K}N$ and $\pi\Sigma$ interactions [27]. In contrast, the $\bar{K}N$ potential in the present investigation is constructed using dimensional regularization of loops in the Bethe-Salpeter equation¹ (see Appendix B for a further detailed assessment of different regularization schemes). The resulting subthreshold amplitudes have significantly smaller real parts in comparison with those using the separable approximation. The reason for this behavior can be traced to the three-momentum form factors commonly used in separable interactions. Standard analytic continuation of the $\bar{K}N$ momentum variable into the subthreshold region lets these form factors increase beyond their threshold (zero-momentum) magnitudes, thereby enhancing the subthreshold amplitude artificially. While such analytic continuations need not be performed in the Faddeev approach, this example nevertheless demonstrates that extrapolations into the far-subthreshold region are confronted with off-shell uncertainties which severely restrict the predictive power of $\bar{K}NN$ binding energy calculations.

Next, we examine the dispersive effect induced by the imaginary part of the $\bar{K}N$ potential. The advantage of the Faddeev method is its ability to deal consistently to all orders with the imaginary parts of the interactions whereas the variational method can handle this only perturbatively. In Section III C we have estimated that dispersive corrections from these imaginary parts amount to about 6 ± 3 MeV binding per nucleon, based on the analysis of the two-body $\bar{K}N$ channel. Thus the dispersive correction to the ppK^- system would add another $\Delta B(ppK^-) \lesssim 15$ MeV to the total binding energy.

On top of these effects, there are several minor differences between two schemes such as the NN potential, admixture of the $|\Phi_- \rangle$ component, and so on. These factors might work together to contribute to the difference between the present result and that in Ref. [20].

We add a short comment on the sensitivity of the ppK^- results to details of the NN potentials. In fact, as long as the $\bar{K}NN$ system is only weakly bound, the dependence on different types of NN interactions is weak. We have performed test calculations using a soft-core potential quite different from Av18 but equivalent with respect to reproducing low-energy NN data. The resulting properties of the ppK^- quasibound system turn out to be very similar to those obtained with the Av18 interaction. Details are given in Appendix D.

¹ This is equivalent to a dispersion relation approach, absorbing uncontrolled high-energy behavior in a few subtraction constants.

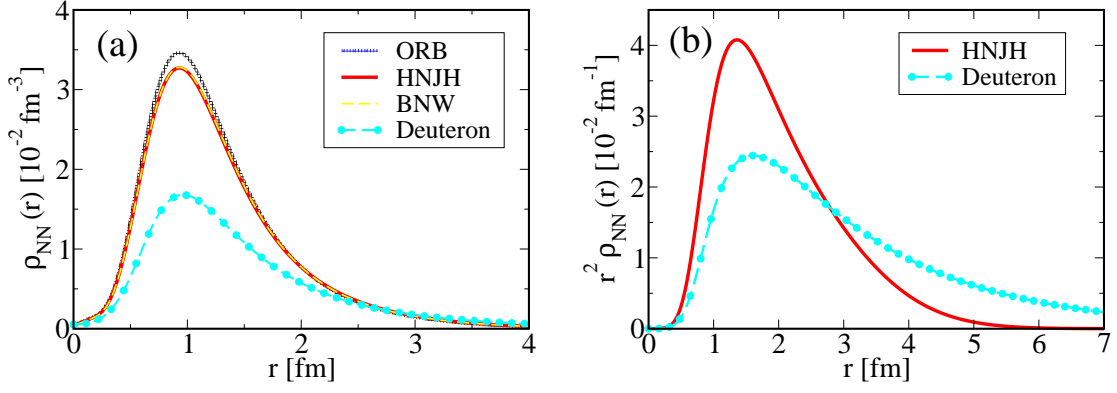


FIG. 3: (Color online) (a) NN density in ppK^- , as function of NN relative distance, calculated with the “Type I” ansatz. “ORB”, “HNJJH” and “BNW” results are shown as crossed, solid and dashed lines, respectively. For comparison, the deuteron density calculated with Av18 potential is depicted as dashed line with filled circle. (b) display of $r^2\rho(r)$ for the same densities.

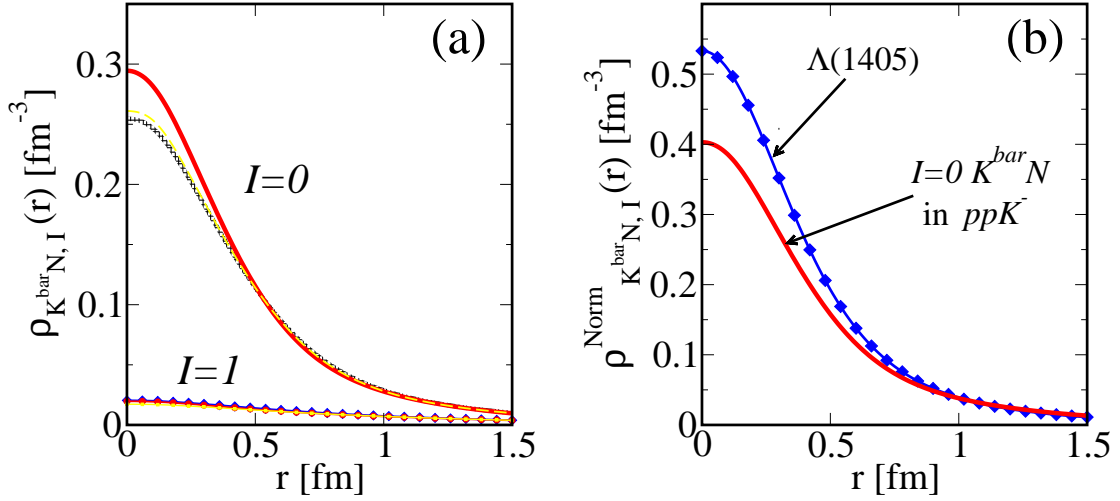


FIG. 4: (Color online) $\bar{K}N$ density in ppK^- , as function of $\bar{K}N$ relative distance, calculated with the “Type I” ansatz. (a) Separate display of each isospin component ($I = 0$ and $I = 1$). Lines without (with) symbols show the $I = 0$ ($I = 1$) component of the $\bar{K}N$ density. Models “ORB”, “HNJJH” and “BNW” are depicted with crossed, solid and dashed lines, respectively. (b) Normalized $I = 0$ $\bar{K}N$ relative density in ppK^- for the model “HNJJH” with the “Type I” ansatz (solid line). Solid line with diamond shows $\bar{K}N$ density in $\Lambda(1405)$ calculated with the same model.

D. Corrections from p -wave $\bar{K}N$ interactions

A rough leading-order estimate of the effect of p -wave $\bar{K}N$ interactions can be performed by computing expectation values of suitably parametrized p -wave K^-p and K^-n potentials. The p -wave $\bar{K}N$ effective potentials used here,

$$v_{\bar{K}N}^{p\text{-wave}}(\mathbf{r}, \sqrt{s}) = -\frac{2C_N(\sqrt{s})}{\sqrt{\pi}a_p^3\tilde{\omega}} \nabla \exp[-\mathbf{r}^2/a_p^2] \nabla, \quad (36)$$

with $\mathbf{r} = \mathbf{r}_{\bar{K}} - \mathbf{r}_N$ and the reduced $\bar{K}N$ energy $\tilde{\omega}$, involve the energy-dependent p -wave scattering “volumes” C_p for K^- -proton and C_n for K^- -neutron, where $C_n \simeq 2C_p$. Their prominent feature is the $\Sigma(1385)$ resonance. We use a parametrization updated from Ref. [41] which has also been used in our previous study [22]. The energy

dependence of C_p is shown in Fig. 5.

Expectation values $\Delta V_{\bar{K}N} = \langle \Psi | v_{\bar{K}N_1}^{p\text{-wave}} + v_{\bar{K}N_2}^{p\text{-wave}} | \Psi \rangle$ of this p -wave $\bar{K}N$ potential are then computed with the ppK^- wave functions of all four chiral models under consideration, changing the range parameter a_p within a reasonable interval, 0.4 fm to 0.9 fm. Then $\text{Re} \Delta V_{\bar{K}N}$ is found to be small and repulsive,

$$1.5 \lesssim \text{Re} \Delta V_{\bar{K}N} \lesssim 5.0 \text{ MeV}. \quad (37)$$

The weak binding of the ppK^- system places the effective \sqrt{s} for the $\bar{K}N$ subsystem above the position of the $\Sigma(1385)$, hence the positive sign of $\text{Re} \Delta V_{\bar{K}N}$. The contribution of p -wave $\bar{K}N$ interactions is small if the ppK^- binding from the driving s -wave interactions is relatively weak as it turns out in the present work. If the binding were strong enough to move the effective energy of the

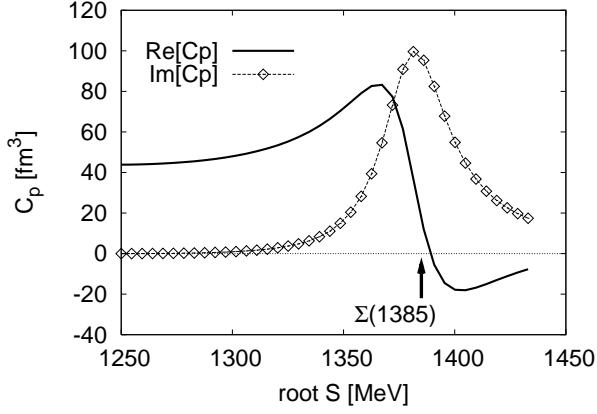


FIG. 5: Energy dependence of K^- -proton scattering volume, C_p . Its real (imaginary) part is drawn with a solid line (dotted line with diamond).

$\bar{K}N$ pair down below the $\Sigma(1385)$ resonance, the p -wave potential would act attractively and would tend to increase the binding. The present results appear to rule out this possibility.

For the correction to the ppK^- width from p -wave $\bar{K}N$ interactions one finds $\Delta\Gamma = -2 \text{Im} \Delta V_{\bar{K}N} \sim 10 - 35 \text{ MeV}$. This relatively large $\Delta\Gamma$ (especially for the type I case) results from the fact that the two-body energy of the $\bar{K}N$ subsystem is located close to the $\Sigma(1385)$ resonance with its prominent imaginary part, see Fig. 5. Obviously we can give here only a rough estimate for orientation.

E. Estimate of antikaon absorption by the two-nucleon pair

A further point of interest is the contribution to the decay width of the ppK^- cluster from the two-body absorption process $K^-pp \rightarrow YN$. This effect is not included in the imaginary part of the $\bar{K}N$ potential used to estimate the decay width (22) in previous sections.

For first guidance, let us start with the formula of the decay width for K^- absorption on proton pairs in a heavy nucleus [42–44]

$$\Delta\Gamma_{abs} = \frac{2\pi\tilde{B}_0}{\omega} \beta_{pp}(\omega) \int d^3\mathbf{r} \rho_{\bar{K}}(\mathbf{r}) \rho_N^2(\mathbf{r}), \quad (38)$$

where ρ_N and $\rho_{\bar{K}}$ are the one-body densities of nucleon and antikaon, $\omega = m_K - B$ is the energy of the meson, and $\beta_{pp}(\omega)$ is a kinematical factor normalized to unity at threshold, $\omega = m_K$ [42, 44]. This factor reflects the phase space and kinematics for the relevant decay chan-

nels (Σ^+n , Σ^0p , and Λp in the present case):

$$\beta_{pp}(\omega) = \sum_{Y=\Lambda,\Sigma} \frac{\alpha_Y}{3} \left(\frac{M(m_K)}{M(\omega)} \right)^3 \times \frac{\sqrt{[M^2(\omega) - m_N^2 + M_Y^2]^2 - 4M^2(\omega)M_Y^2}}{\sqrt{[M^2(m_K) - m_N^2 + M_Y^2]^2 - 4M^2(m_K)M_Y^2}}$$

where $M(\omega) = 2M_N + \omega$ and $\alpha_\Lambda = 1$, $\alpha_\Sigma = 2$. Eq. (38) derives from an effective contact interaction, with the coupling strength \tilde{B}_0 estimated empirically as $\tilde{B}_0 \sim 1 \text{ fm}^4$ [44] on the basis of kaonic atom data summarized and discussed in Refs. [42, 43].

The absorptive width in the form (38) is proportional to the probability of finding three particles (antikaon and two nucleons) at the same space point, as expressed by the product of the one-body densities. This treatment is justified for large nuclei where the independent particle picture works reasonably well. However, for the few-body K^-pp system, the following modifications are required:

- (i) correlations between the two nucleons must be taken into account, and
- (ii) finite range effects in the absorption process must be considered.

The first modification is mandatory because of the repulsive core in the nucleon-nucleon interaction. Once the correlations are taken into account, a local absorptive contact interaction (38) is not appropriate because it provides almost no width: the probability for two nucleons to be found at the same spot is basically zero. A proper treatment must therefore deal with finite range effects in the absorption process which in turn requires a more detailed assessment of the underlying microscopic mechanisms.

By analogy with pion absorption in the deuteron, a leading microscopic process would be one-pion exchange (Fig. 6, left). This process, however, does not contribute to K^- absorption on a proton-proton pair with spin $S = 0$ in the K^-pp system considered here. So the driving absorption mechanism is expected to come from exchanges of two pseudoscalar mesons as illustrated in Fig. 6. In chiral effective field theory, these are subleading one-loop terms in the two-baryon system involving $\bar{K}\pi\pi$ or $\bar{K}K\pi$ couplings to one of the baryons and exchange of the (interacting) two mesons with the second baryon. These processes occur when the external antikaon overlaps with one of the nucleons. The effective range of the absorption process is then related to the mass spectrum representing the exchanged two-meson system.

Thus, in order to estimate the width from the two-nucleon absorption process, we need to extend the formula (38) to satisfy the requirements (i) and (ii). The result should reduce to the original form (38) in the limit of no NN correlations and zero-range interaction, so that contacts to phenomenology can be made concerning the absorptive coupling strength \tilde{B}_0 .

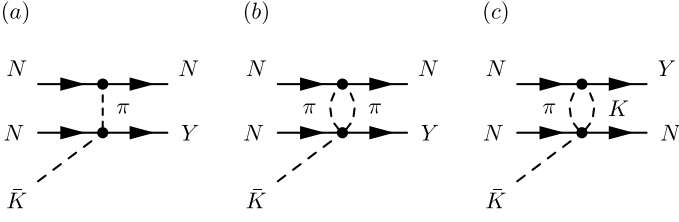


FIG. 6: Feynman diagrams for typical microscopic mechanisms of the two-nucleon absorption process. (a): one pion exchange which is forbidden in the present system, (b) and (c): two-meson exchange.

First note that the product of one-body densities can be expressed as

$$\rho_{\bar{K}}(\mathbf{r})\rho_N^2(\mathbf{r}) = \int d^3\mathbf{x}_1 \int d^3\mathbf{x}_2 \rho_{\bar{K}}(\mathbf{r}) \rho_N(\mathbf{x}_1) \rho_N(\mathbf{x}_2) \times \delta^3(\mathbf{x}_1 - \mathbf{x}_2) \sum_{i=1,2} \frac{\delta^3(\mathbf{x}_i - \mathbf{r})}{2}. \quad (39)$$

For the modification requested by item (i), we introduce the three-body density as

$$\begin{aligned} \rho^{(3)}(\mathbf{r}, \mathbf{x}_1, \mathbf{x}_2) \\ \equiv \langle \Psi | \delta^3(\mathbf{r}_{\bar{K}} - \mathbf{r}) \delta^3(\mathbf{r}_1 - \mathbf{x}_1) \delta^3(\mathbf{r}_2 - \mathbf{x}_2) | \Psi \rangle \\ = \rho_{\bar{K}}(\mathbf{r}) \rho_N(\mathbf{x}_1) \rho_N(\mathbf{x}_2) [1 - C(\mathbf{r}, \mathbf{x}_1, \mathbf{x}_2)], \end{aligned}$$

where the function $C(\mathbf{r}, \mathbf{r}_1, \mathbf{r}_2)$ represents the correlations among the particles. The product of one-body densities in Eq. (39) can now be replaced by the three-body density $\rho^{(3)}(\mathbf{r}, \mathbf{x}_1, \mathbf{x}_2)$ which reduces to the original form in the limit of $C \rightarrow 0$. The modification (ii) is implemented by replacing the delta function in Eq. (39) by a finite range distribution, such as a normalized Gaussian:

$$\delta^3(\mathbf{x}_1 - \mathbf{x}_2) \rightarrow G(\mathbf{x}_1 - \mathbf{x}_2; a) = \frac{1}{\pi^{3/2} a^3} e^{-|\mathbf{x}_1 - \mathbf{x}_2|^2/a^2}.$$

Taking $a \rightarrow 0$, this distribution turns into the delta function. In summary, the formula for the absorptive width of the ppK^- few-body system is given by

$$\begin{aligned} \Delta\Gamma_{abs}(K^- pp \rightarrow YN) = \frac{2\pi B_0}{\omega} \beta_{pp}(\omega) \\ \times \int d^3\mathbf{r} \int d^3\mathbf{x} \rho^{(3)}(\mathbf{r}, \mathbf{r}, \mathbf{x}) G(\mathbf{x} - \mathbf{r}; a). \quad (40) \end{aligned}$$

The variation of $\Delta\Gamma_{abs}$ with respect to changes of the Gaussian range parameter a is shown in Fig. 7. Note that, from the point of view of the microscopic $\pi\pi$ or πK exchange mechanisms discussed previously, the characteristic ranges are covering a band from $a \sim 0.4$ fm for K^* exchange to about $a \sim 1.4$ fm for uncorrelated 2π exchange. For a typical choice of the absorptive coupling strength, $\bar{B}_0 = 1$ fm⁴ and $a = 0.6$ fm, one finds:

$$5 \text{ MeV} \lesssim \Delta\Gamma_{abs} \lesssim 8 \text{ MeV} \quad (41)$$

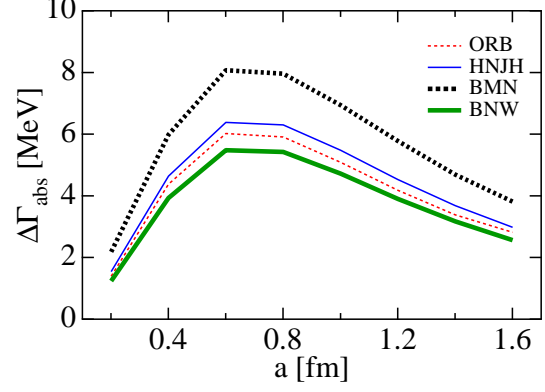


FIG. 7: (Color online) Absorptive width $\Delta\Gamma_{abs}$ for $ppK^- \rightarrow YN$ as function of Gaussian range parameter a . Results are shown for the models ‘‘ORB’’, ‘‘HNJH’’, ‘‘BNW’’ and ‘‘BMN’’ discussed in the text.

for all models (with Type I or Type II ansatz). The coupling strength \bar{B}_0 is, of course, subject to considerable uncertainties. From the recent survey [43] based on kaonic atom data analysis one estimates a possible band width $0.85 < \bar{B}_0 < 1.5$ fm⁴ [44] which translates into

$$4 \text{ MeV} \lesssim \Delta\Gamma_{abs} \lesssim 12 \text{ MeV}. \quad (42)$$

Given this estimated upper limit for $\Delta\Gamma_{abs}$ in the ppK^- system we conclude that the absorptive width in such a dilute, weakly bound system is expected to be less important than the one from the mesonic $\bar{K}NN \rightarrow \pi YN$ decay under the given conditions. This situation may change qualitatively for heavier nuclei with potentially stronger \bar{K} binding where the absorptive width can be far more prominent as pointed out in Ref. [44].

V. SUMMARY

We have investigated the prototype of antikaonic nuclei, ppK^- , using a variational approach with an effective $\bar{K}N$ interaction derived from chiral SU(3) coupled-channel dynamics. Several versions of such $\bar{K}N$ interactions have been employed in the calculations. They all satisfy the necessary constraint of reproducing empirical K^-p threshold information and the $\pi\Sigma$ mass spectrum in the region of the $\Lambda(1405)$, within (admittedly large) uncertainties of the existing experimental data base. Furthermore, a realistic nucleon-nucleon interaction (Argonne v18) has been used throughout. This interaction properly accounts for repulsive short-distance NN correlations.

The primary problem faced in the theoretical part of the quest for antikaon-nuclear quasibound systems is the subthreshold extrapolation of the s -wave $\bar{K}N$ interaction. As a consequence of the strong $\bar{K}N \leftrightarrow \pi\Sigma$ coupled-channel dynamics, this interaction is complex, non-local

and energy dependent. While the driving interaction kernel is determined by chiral SU(3) dynamics, the off-shell extrapolation into the far-subthreshold region is subject to uncertainties which limit the predictive power of the theory. A minimal condition for any such calculation is to account in detail for the coupled-channel dynamics that governs the formation of the $\Lambda(1405)$ as a quasi-bound $\bar{K}N$ state embedded in the strongly interacting, resonant $\pi\Sigma$ continuum. When this is done, the resulting $\bar{K}N$ effective potential turns out to be significantly less attractive than anticipated in a simple phenomenological approach using a local, energy-independent potential. As a consequence we arrive at weaker ppK^- binding than that previously suggested.

As an independent test of the variational method applied in the present investigation, we have performed calculations using the phenomenological Akaishi-Yamazaki (AY) potential. The stronger binding found with this energy independent local potential is indeed reproduced as reported in detail in Appendix C.

The results of the present variational calculation are summarized as follows:

- The calculated binding energy of the ppK^- cluster, based on the leading s -wave $\bar{K}N$ interaction only, is

$$B(ppK^-) \simeq 20 \pm 3 \text{ MeV} ,$$

where the error indicates variations using four different versions of chiral SU(3) coupled-channel calculations. The decay width into πYN final states is estimated to be in the range

$$\Gamma(ppK^- \rightarrow \pi YN) \sim 40 - 70 \text{ MeV} .$$

- Differences between these variational results and those obtained from Faddeev calculations [20] presumably relate in large part to $\pi\Sigma N$ three-body dynamics not incorporated in the present framework. Some part of these differences may be attributed to the use of separable approximations for the $\bar{K}N$ and πY interactions when solving Faddeev equations, and to dispersive effects not covered by the variational approach. We estimate the dispersive correction to the total ppK^- binding energy to be $\Delta B(ppK^-) \lesssim 15 \text{ MeV}$.
- This additional binding is partly compensated by corrections from p -wave $\bar{K}N$ interactions which have a repulsive effect as long as the effective two-body energy in the $\bar{K}N$ subsystem stays above the $\Sigma(1385)$ resonance. The overall binding energy, after corrections and with conservative error assignment, is then expected to be in the interval $B(ppK^-) \simeq 20 - 40 \text{ MeV}$.
- The p -wave interactions tend to increase the mesonic decay width for $ppK^- \rightarrow \pi YN$ by an amount of 10 - 35 MeV.

- The additional effects of $\bar{K}NN \rightarrow YN$ absorption are estimated to increase the decay width of the quasibound ppK^- state further by an amount of order 10 MeV.
- In the variational approach the wave function of the ppK^- quasibound state can be computed and analyzed. Given its weak binding, the system is rather dilute. The average distance between the two nucleons is about 2.1 - 2.2 fm. The short-range repulsion in the NN interaction plays an important role in keeping the nucleons apart. The antikaon likes to minimize its distance from either nucleon. The isospin $I = 0$ $\bar{K}N$ density distribution within the $\bar{K}NN$ cluster is reminiscent of the $\Lambda(1405)$ in the $\bar{K}N$ two-body system, indicating a $\Lambda(1405)N$ dibaryonic hybrid structure. However, with its estimated lifetime of order $\tau = 1/\Gamma \sim 2 \text{ fm}/c$, this structure can exist only over a very short time interval.

Taking all theoretical uncertainties into account, we arrive at the conclusion that narrow, deeply bound ppK^- clusters are unlikely to exist. Our calculation predicts such systems to be weakly bound and short-lived. With a rather low binding energy and a total width between 60 and 120 MeV, such structures would indeed be difficult to detect. One should keep in mind, however, that the present calculations rely entirely on the constraints provided by the presently available sets of K^-p threshold data and the poorly known $\pi\Sigma$ mass spectrum. Improvements of this data base will sharpen the theoretical input conditions for deriving the effective subthreshold $\bar{K}N$ interaction. One can look forward to further developments along these lines as the experimental searches proceed with higher precision.

ACKNOWLEDGEMENTS

We thank Avraham Gal for fruitful and stimulating discussions. One of authors (A. D.) is grateful to Prof. Akaishi for advice on the construction of our model wave function. This project is partially supported by BMBF, GSI and by the DFG excellence cluster "Origin and Structure of the Universe". T. H. thanks the Japan Society for the Promotion of Science (JSPS) for financial support. This work is also supported in part by the Grant for Scientific Research (No. 19853500, 19740163) from the Ministry of Education, Culture, Sports, Science and Technology (MEXT) of Japan. This research is part of Yukawa International Program for Quark-Hadron Sciences.

APPENDIX A: NN POTENTIALS

For practical convenience in performing the variational calculations, the original Av18 potential has been repre-

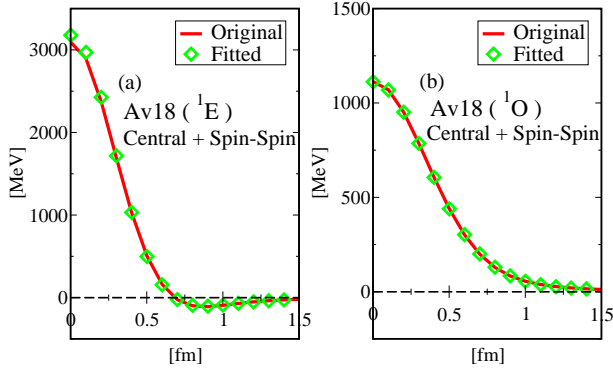


FIG. 8: (Color online) Central plus spin-spin NN potentials in singlet-even (a) and singlet-odd (b) channels. Solid line: original Argonne v18 potential (“Original”). Points represent fits to the original potential with four Gaussians (“Fitted”).

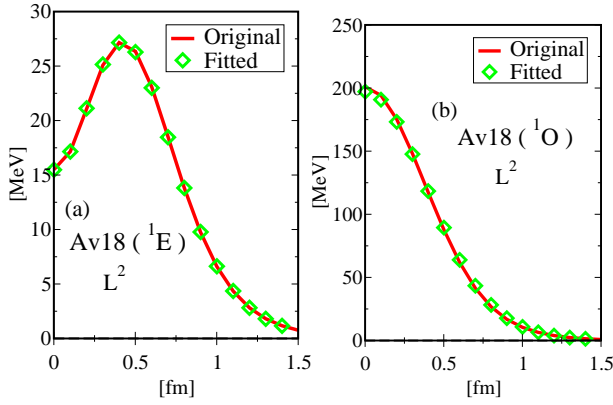


FIG. 9: (Color online) L^2 potential in NN potential. Figs. (a) and (b) show 1E and 1O channels, respectively. Solid line is the original Argonne v18 potential (“Original”). Points represent the potential used in the present study, which fit the original potential with three Gaussians (“Fitted”).

sented by a series of Gaussians.

The spin state of the two nucleons is restricted to $S = 0$ in our model, so the expectation value of the operator $\hat{\sigma}_1 \cdot \hat{\sigma}_2$ in the spin-spin potential is equal to -3 . We have fitted the radial parts of the central potential plus the spin-spin potential, $v_X^c(r) - 3v_X^{SS}(r)$, with four Gaussians of different ranges; the radial part of L^2 potential, $v_X^{L^2}(r)$, is fitted with three Gaussians:

$$v_X^c(r) - 3v_X^{SS}(r) = \sum_{n=1}^4 v_n^{c+SS,X} e^{-(r/r_n^{c+SS,X})^2}, \quad (\text{A1})$$

$$v_X^{L^2}(r) = \sum_{n=1}^3 v_n^{L^2,X} e^{-(r/r_n^{L^2,X})^2}, \quad (\text{A2})$$

with strengths $v_n^{c+SS,X}$ and $v_n^{L^2,X}$ and ranges $r_n^{c+SS,X}$ and $r_n^{L^2,X}$, where X indicates the channels 1E , 1O . The values of the parameters are listed in Table V. For illustration of the fit quality we draw the potentials in Figs. 8 and 9.

TABLE V: Best fit parameters for the expansion of the Av18 potential into Gaussians. Strengths are given in MeV, ranges in fm.

n	1	2	3	4
$v_n^{c+SS,1E}$	3708	-483	-44	-3
$r_n^{c+SS,1E}$	0.411	0.726	1.317	2.619
$v_n^{c+SS,1O}$	651	412	43	6
$r_n^{c+SS,1O}$	0.453	0.603	1.092	2.622
$v_n^{L^2,1E}$	-47	57	5	
$r_n^{L^2,1E}$	0.383	0.637	1.009	
$v_X^{L^2,1O}$	170	27	-0.3	
$r_X^{L^2,1O}$	0.537	0.804	1.644	

APPENDIX B: CHIRAL COUPLED-CHANNEL APPROACH AND REGULARIZATION DEPENDENCE

Here we briefly summarize basics of the chiral $SU(3)$ coupled-channel approach [26]. In particular, we study the regularization dependence of the $\bar{K}N$ and $\pi\Sigma$ amplitudes, an issue that has repeatedly been raised in the literature.

The starting point is the coupled-channel meson-baryon scattering equation

$$T_{ij} = V_{ij} + V_{ik} G_k T_{kj}, \quad (\text{B1})$$

with the interaction kernel V_{ij} derived from the chiral $SU(3)$ meson-baryon Lagrangian, and the loop function G_k to be discussed in detail later. In order to derive the single-channel $\bar{K}N$ potential, an effective interaction kernel V^{eff} is constructed such that the full solution of Eq. (B1) in the $\bar{K}N$ channel is reproduced by solving a single-channel scattering equation with V^{eff} :

$$T_{11} = V^{\text{eff}} + V^{\text{eff}} G_1 T_{11}, \quad (\text{B2})$$

where $i = j = 1$ now represents the $\bar{K}N$ channel. This V^{eff} is used in Eq. (26) to determine the strength of the $\bar{K}N$ potential.

In Ref. [26], dimensional regularization was used in the calculation of the loop function G . Dimensional regularization has the advantage that the analyticity of the loop function is compatible with the dispersion relation used in the N/D method [29]. It is however instructive to study the regularization dependence in this framework, in order to understand possible differences between present results for the K^-pp system and the results of the Faddeev calculation with interactions constrained by chiral dynamics [20]. An analysis of the regularization dependence in this framework can be found in Ref. [45]. Note that differences in the regularization schemes only change

the loop function G and leave the interaction kernel V untouched.

Using dimensional regularization, the loop function G is given by

$$G^{dim}(\sqrt{s}) = \frac{2M}{(4\pi)^2} \left\{ a(\mu) + \ln \frac{mM}{\mu^2} + \frac{\Delta}{s} \ln \frac{M}{m} + \frac{\bar{q}}{\sqrt{s}} \ln \frac{\phi_{++}(s)\phi_{+-}(s)}{\phi_{-+}(s)\phi_{--}(s)} \right\}, \quad (\text{B3})$$

where $a(\mu)$ are subtraction constants, μ is the renormalization scale, and we have defined

$$\begin{aligned} \Delta &= M^2 - m^2, \\ \phi_{\pm\pm}(s) &= \pm s \pm \Delta + 2\bar{q}\sqrt{s}, \\ \bar{q} &= \frac{\sqrt{(s - (M - m)^2)(s - (M + m)^2)}}{2\sqrt{s}}. \end{aligned}$$

With a sharp three-momentum cutoff, the loop function is

$$G^{3d}(\sqrt{s}) = \frac{2M}{(4\pi)^2} \left\{ \ln \frac{mM}{q_{\max}^2} + \frac{\Delta}{s} \ln \frac{M(1 + \xi^m)}{m(1 + \xi^M)} - \ln [(1 + \xi^m)(1 + \xi^M)] + \frac{\bar{q}}{\sqrt{s}} \ln \frac{\phi_{+}^m(s)\phi_{+}^M(s)}{\phi_{-}^m(s)\phi_{-}^M(s)} \right\}, \quad (\text{B4})$$

where q_{\max} is the three-momentum cutoff and

$$\begin{aligned} \phi_{\pm}^m(s) &= \pm s \mp \Delta + 2\bar{q}\sqrt{s}\xi^m, \\ \phi_{\pm}^M(s) &= \pm s \pm \Delta + 2\bar{q}\sqrt{s}\xi^M, \\ \xi^m &= \sqrt{1 + \frac{m^2}{q_{\max}^2}}, \quad \xi^M = \sqrt{1 + \frac{M^2}{q_{\max}^2}}. \end{aligned}$$

A smooth cutoff can be introduced using the Pauli-Villars method which corresponds to multiplying a monopole form factor

$$\frac{m^2 - \Lambda^2}{q^2 - \Lambda^2}$$

to the loop function, leading to

$$G^{PV}(\sqrt{s}) = \frac{2M}{(4\pi)^2} \left\{ \ln \frac{m}{\Lambda} + \frac{\Delta}{s} \ln \frac{M}{m} - \frac{\Delta_{\Lambda}}{s} \ln \frac{M}{\Lambda} + \frac{\bar{q}}{\sqrt{s}} \ln \frac{\phi_{++}(s)\phi_{+-}(s)}{\phi_{-+}(s)\phi_{--}(s)} - \frac{\bar{q}_{\Lambda}}{\sqrt{s}} \ln \frac{\phi_{\Lambda,++}(s)\phi_{\Lambda,+}(s)}{\phi_{\Lambda,-+}(s)\phi_{\Lambda,--}(s)} \right\}, \quad (\text{B5})$$

where

$$\begin{aligned} \Delta_{\Lambda} &= M^2 - \Lambda^2, \\ \phi_{\Lambda,\pm\pm}(s) &= \pm s \pm \Delta_{\Lambda} + 2\bar{q}_{\Lambda}\sqrt{s}, \\ \bar{q}_{\Lambda} &= \frac{\sqrt{(s - (M - \Lambda)^2)(s - (M + \Lambda)^2)}}{2\sqrt{s}} \end{aligned}$$

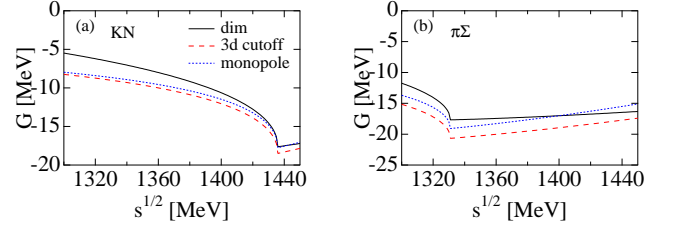


FIG. 10: (Color online) Comparison of the loop functions: dimensional regularization (solid lines), three-momentum sharp cutoff (dashed lines), and smooth monopole form factor (dotted lines). (a): $\bar{K}N$ channel, (b): $\pi\Sigma$ channel.

The real parts of the loop functions (B3), (B4), and (B5) for $\bar{K}N$ and $\pi\Sigma$ channels are plotted in Fig. 10. The imaginary parts are determined by the phase space of intermediate meson-baryon states and therefore independent of the regularization procedure. The parameters for the dimensional regularization and three momentum cutoff schemes are taken from phenomenologically successful models [28, 36]:

$$\begin{aligned} a_{\bar{K}N} &= -2, \quad a_{\pi\Sigma} = -1.84, \quad \mu = 630 \text{ MeV}, \\ q_{\max} &= 630 \text{ MeV}. \end{aligned}$$

The loop functions G^{dim} and G^{3d} are evidently quite similar. Furthermore, choosing the parameter of the monopole form factor as

$$\Lambda_{\bar{K}N} = 750 \text{ MeV}, \quad \Lambda_{\pi\Sigma} = 500 \text{ MeV}$$

the corresponding loop functions G^{PV} behave quantitatively similar as those with dimensional/three-momentum cutoff schemes, as seen in Fig. 10. The cutoff scales of the form factors (several hundreds of MeV) is typical and naturally expected from meson-baryon phenomenology.

In summary, we find that smooth cutoff schemes provide similar loop functions as those with sharp cutoff or dimensional regularization. Since differences in the regularization schemes only affect the loop functions G in the present framework, it is clear that the potentials derived in Ref. [26] remain unchanged when adopting a smooth cutoff.

In this respect, the difference between the present results for K^-pp binding and those in Faddeev method [20] cannot be attributed to the regularization method. It is worth noting that early studies using the coupled-channel approach [27] gave a stronger \bar{K} subthreshold amplitude than the one derived in Ref. [26]. The calculations of Ref. [27] used a separable approximation for the potential together with the non-relativistic Lippmann-Schwinger equation, a feature also shared by the Faddeev calculations of Ref. [20]. Thus the larger binding energy of K^-pp found in Ref. [20] is likely to be related to the type of scattering equation and the separable approximation used in that work.

TABLE VI: Test of the present variational calculation with the AY potential [21]. “Model I” and “Model II” are the results using the variational wave function described in Sec. II A. “ATMS” refers to the results quoted in Ref. [21]. $B(ppK^-)$ and Γ are the total ppK^- binding energy and the $\bar{K}NN \rightarrow \pi YN$ decay width. The antikaon binding energy B_K is defined in Eq. (16). All the remaining quantities are specified as in Table III. All energies are given in units of MeV. The r.m.s. distances R_{NN} and $R_{\bar{K}N}$ are in fm.

C	Model I 0	Model II finite	ATMS —
$B(ppK^-)$	39.0	51.4	48
Γ	60.0	61.0	61
B_K	65.8	80.0	68
T_{nuc}	46.7	47.8	—
E_{kin}	147.0	162.4	167
$V(NN)$	-19.8	-19.2	-19
$V(\bar{K}N)$	-166.2	-194.6	-196
R_{NN}	1.75	1.83	1.90
$R_{\bar{K}N}$	1.54	1.55	1.57
$P(T_N = 0)$	0	5.9 %	—

APPENDIX C: BENCHMARK TEST WITH THE AY POTENTIAL

As a test for the variational method and trial wave functions applied in the present work, we perform a calculation with the $\bar{K}N$ interaction [the Akaishi-Yamazaki (AY) potential] and the NN interaction (the Tamagaki potential) used in Ref.[21]. The AY potential is an energy-independent, local potential based on phenomenology but not constrained by chiral SU(3) dynamics.

The results are summarized in Table VI. The first two columns (“Model I” and “Model II”) show our results; the last column (“ATMS”) is the original result reported in Ref. [21]. In “Model I” the energy variation is performed restricting the wave function to its dominant $|\Phi_+\rangle$ component, i.e. with no admixture of the $|\Phi_-\rangle$ state (the one with NN coupled to isospin $T_N = 0$), keeping the coefficient $C \equiv 0$ in Eq.(1). “Model II” includes the $|\Phi_-\rangle$ component, with C determined variationally. In all calculations, the convergence of the Gaussian expansions (6) and (7) has been checked and found satisfactory with $N_N = N_K = 9$.

One evidently finds a high degree of consistency between “Model II” and “ATMS”, confirming that the different variational methods used here and in Ref. [21] are of comparable quality.

The importance of the $T_N = 0$ component of the wave function is underlined by the comparison between “Model I” with “Model II”. Although this admixture is only

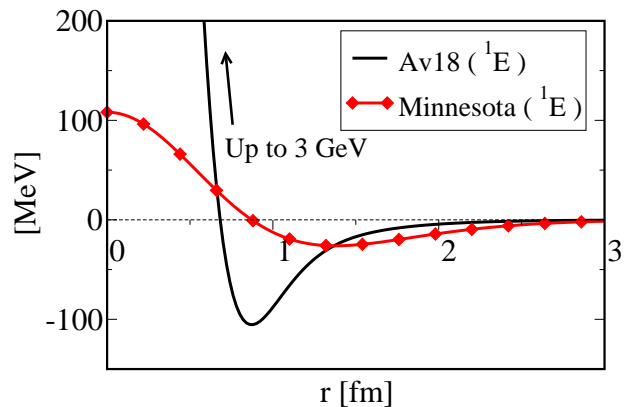


FIG. 11: (Color online) Comparison of Minnesota potential with Av18 potential. 1E channel of both potentials are shown. Minnesota potential is depicted with a solid line with diamond. Av18 potential is depicted with a solid line.

about 6 % as shown in the last row [$P(T_N = 0)$] in Table VI, switching it off reduces the binding energy by more than 20 %. The matrix elements of the $\bar{K}N$ interaction taken between normalized states $|\Phi_+\rangle$ and $|\Phi_-\rangle$ are as follows:

$$\langle \Phi_+ | \hat{V}_{\bar{K}N} | \Phi_+ \rangle = \frac{3}{4} v_{\bar{K}N}^{I=0} + \frac{1}{4} v_{\bar{K}N}^{I=1}, \quad (C1)$$

$$\langle \Phi_- | \hat{V}_{\bar{K}N} | \Phi_- \rangle = \frac{1}{4} v_{\bar{K}N}^{I=0} + \frac{3}{4} v_{\bar{K}N}^{I=1}, \quad (C2)$$

$$\langle \Phi_+ | \hat{V}_{\bar{K}N} | \Phi_- \rangle = \frac{\sqrt{3}}{4} (v_{\bar{K}N}^{I=0} - v_{\bar{K}N}^{I=1}). \quad (C3)$$

The mixture implied by Eq. (C3) increases the ppK^- binding energy. For the AY potential the values of these three matrix elements are -173.3 MeV, -112.3 MeV and -53.0 MeV, in this order. Taking the mixing ratio between $|\Phi_+\rangle$ and $|\Phi_-\rangle$ into account, the actual contributions from each matrix element to the $\bar{K}N$ potential energy are -163.1 MeV, -6.6 MeV and -24.9 MeV, respectively, and so the coupling matrix element (C3) is found to be attractive and non-negligible.

In concluding this Appendix we note again that the overall attraction produced by the $\hat{V}_{\bar{K}N}$ based on chiral SU(3) dynamics, and used in the present work, is considerably weaker in comparison and leads to a ppK^- binding energy less than half of that found with the simple AY potential.

APPENDIX D: DEPENDENCE ON THE NN POTENTIAL

Test calculations have been performed replacing the Av18 by a soft-core NN potential, the Minnesota potential [46] (see Fig. 11). This potential reproduces low-energy NN data (scattering lengths, effective ranges, and deuteron properties) just like the more realistic Av18 interaction. In the actual computations, we have fixed a

TABLE VII: Dependence of ppK^- results on the NN potential. The first and second lines indicate the type of $\bar{K}N$ and NN potential, respectively. “Minnesota” in the second line refers to the soft-core potential of Ref. [46]. E_{nuc} is the total energy of nuclear part, namely $E_{nuc} = T_{nuc} + V(NN)$. Other quantities shown in this table are the same as those in Table VI. All results are obtained with Gaussian expansions $N_N = N_K = 5$ in Eqs. (6) and (7).

$\bar{K}N$	HNJH		AY	
NN	Av18	Minnesota	Av18	Minnesota
$B(ppK^-)$	16.9	17.0	49.0	50.4
Γ	47.0	49.4	60.1	64.7
B_K	38.9	42.1	78.1	84.2
E_{nuc}	22.0	25.1	29.1	33.8
T_{nuc}	38.1	32.9	49.5	41.3
E_{kin}	129.5	131.3	160.6	160.0
$V(NN)$	-16.2	-7.8	-20.5	-7.5
$V(\bar{K}N)$	-130.4	-140.5	-189.2	-202.9
R_{NN}	2.21	2.15	1.82	1.80
$R_{\bar{K}N}$	1.97	1.93	1.56	1.53
$P(T_N = 0)$	3.8 %	4.5 %	4.4 %	5.1 %

parameter of the Minnesota potential ($u = 1$) so that it corresponds to a Serber-type potential.

Results of ppK^- calculations are summarized in Table VII for the chiral $\bar{K}N$ potential (HNJH) and for the phenomenological AY potential. The sensitivity to details of the NN interaction turns out to be marginal for the weakly bound ppK^- system and slightly more pronounced but still weak for the more strongly bound AY case. The qualitative difference between strong and soft

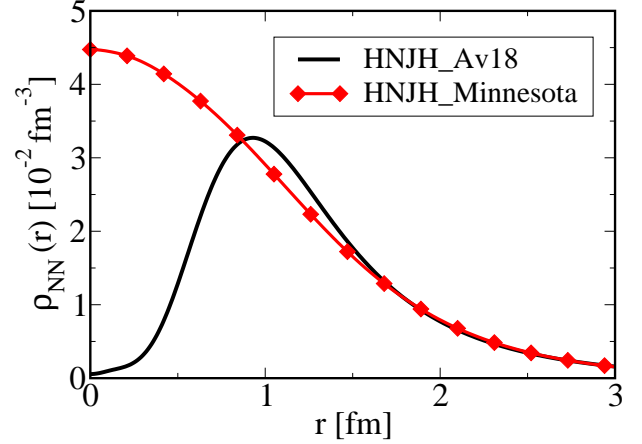


FIG. 12: (Color online) NN density for Av18 potential (solid line) and Minnesota potential (solid line with diamond). A chiral-based $\bar{K}N$ potential (HNJH) is used.

short-range repulsive core becomes apparent, however, when examining the NN density distribution within the $\bar{K}NN$ clusters (see Fig. 12).

- [1] D. B. Kaplan and A. E. Nelson, Phys. Lett. **B175**, 57 (1986).
- [2] D. B. Kaplan and A. E. Nelson, Nucl. Phys. **A479**, 273 (1988).
- [3] G. E. Brown, C. H. Lee, M. Rho, and V. Thorsson Nucl. Phys. **A567**, 937 (1994).
- [4] T. Waas, N. Kaiser, and W. Weise, Phys. Lett. **B379**, 34 (1996).
- [5] T. Waas and W. Weise, Nucl. Phys. **A625**, 287 (1997).
- [6] T. Waas, M. Rho, and W. Weise, Nucl. Phys. **A617**, 449 (1997).
- [7] M. F. M. Lutz and C. L. Korpa Nucl. Phys. **A700**, 309 (2002); M. F. M. Lutz, C. L. Korpa and M. Moller, Nucl. Phys. A **808**, 124 (2008).
- [8] Y. Akaishi and T. Yamazaki, Phys. Rev. C **65**, 044005 (2002); T. Yamazaki and Y. Akaishi, Phys. Lett. **B535**, 70 (2002).
- [9] A. Doté, H. Horiuchi, Y. Akaishi and T. Yamazaki, Phys. Lett. **B590**, 51 (2004); Phys. Rev. C **70**, 044313 (2004).
- [10] T. Suzuki *et al.*, Phys. Lett. **B597**, 263 (2004).
- [11] T. Kishimoto *et al.*, Prog. Theor. Phys. Suppl. **149**, (2003) 264; Nucl. Phys. **A754**, 383 (2005).
- [12] M. Agnello *et al.*, (FINUDA collaboration), Phys. Rev. Lett. **94**, 212303 (2005).
- [13] T. Kishimoto *et al.*, Prog. Theor. Phys. **118**, 181 (2007).
- [14] M. Agnello *et al.*, Nucl. Phys. **A775**, 35 (2006).
- [15] M. Sato *et al.*, Phys. Lett. **B659**, 107 (2008).
- [16] T. Suzuki *et al.*, Phys. Rev. C **76**, 068202 (2007).
- [17] T. Suzuki *et al.*, arXiv:0711.4943 [nucl-ex].
- [18] V. K. Magas, E. Oset, A. Ramos and H. Toki, Phys. Rev. C **74**, 025206 (2006); V. K. Magas, E. Oset and A. Ramos, Phys. Rev. C **77**, 065210 (2008).
- [19] N. V. Shevchenko, A. Gal, and J. Mares, Phys. Rev. Lett. **98**, 082301 (2007); N. V. Shevchenko, A. Gal, J. Mares, and J. Révai, Phys. Rev. C **76**, 044004 (2007).
- [20] Y. Ikeda and T. Sato, Phys. Rev. C **76**, 035203 (2007).
- [21] T. Yamazaki and Y. Akaishi, Phys. Rev. C **76**, 045201 (2007).
- [22] A. Doté and W. Weise, Prog. Theor. Phys. Suppl. **168**, 593 (2007); A. Doté and W. Weise, nucl-th/0701050, in: Proceedings HYP06, “Hypernuclear and Strange Particle Physics”, J. Pochodzalla and Th. Walcher, ed., p 249, Springer, Heidelberg, 2007 (ISBN 978-3-540-76365-9).
- [23] A. Arai, M. Oka and S. Yasui, Prog. Theor. Phys. **119**, 103 (2008).
- [24] A. Doté, T. Hyodo and W. Weise, Nucl. Phys. **A804**, 197 (2008).
- [25] T. Koike and T. Harada, Phys. Lett. **B652**, 262 (2007); Nucl. Phys. **A804**, 231 (2008).
- [26] T. Hyodo and W. Weise, Phys. Rev. C **77**, 035204 (2008).
- [27] N. Kaiser, P. B. Siegel, and W. Weise, Nucl. Phys. **A594**, 325 (1995); N. Kaiser, T. Waas, and W. Weise, Nucl.

- Phys. **A612**, 297 (1997); J. Caro Ramon, N. Kaiser, S. Wetzel, and W. Weise, Nucl. Phys. **A672**, 249 (2000).
- [28] E. Oset and A. Ramos, Nucl. Phys. **A635**, 99 (1998).
- [29] J. A. Oller and U. G. Meissner, Phys. Lett. **B500**, 263 (2001).
- [30] M. F. M. Lutz and E. E. Kolomeitsev, Nucl. Phys. **A700**, 193 (2002).
- [31] B. Borasoy, R. Nissler, and W. Weise, Phys. Rev. Lett. **94**, 213401 (2005).
- [32] R. H. Dalitz, T. C. Wong and G. Rajasekaran, Phys. Rev. **153** (1967) 1617.
- [33] P. B. Siegel and W. Weise, Phys. Rev. C **38**, 2221 (1988).
- [34] *Numerical Recipes in Fortran 77*, 2nd Edition, Chapter 10.4, p. 402, Cambridge Univ. Press (ISBN 0-521-43064-X).
- [35] R. B. Wiringa, V. G. J. Stoks and R. Schiavilla, Phys. Rev. C **51**, 38 (1995).
- [36] E. Oset, A. Ramos, and C. Bennhold, Phys. Lett. **B527**, 99 (2002).
- [37] T. Hyodo, S. I. Nam, D. Jido, and A. Hosaka, Phys. Rev. C **68**, 018201 (2003); Prog. Theor. Phys. **112**, 73 (2004).
- [38] B. Borasoy, R. Nissler, and W. Weise, Eur. Phys. J. A **25**, 79 (2005).
- [39] B. Borasoy, U. G. Meissner, and R. Nissler, Phys. Rev. C **74**, 055201 (2006).
- [40] T. Sekihara, T. Hyodo and D. Jido, Phys. Lett. **B669**, 133 (2008); Mod. Phys. Lett. A **23**, 2412-2424 (2008).
- [41] R. Brockmann, W. Weise and L. Tauscher, Nucl. Phys. **A308**, 365 (1978).
- [42] J. Mares, E. Friedman and A. Gal, Nucl. Phys. A **770**, 84 (2006).
- [43] E. Friedman and A. Gal, Phys. Rept. **452**, 89 (2007).
- [44] W. Weise and R. Härtle, Nucl. Phys. **A804**, 173 (2008).
- [45] S. I. Nam, H. C. Kim, T. Hyodo, D. Jido and A. Hosaka, J. Korean Phys. Soc. **45**, 1466 (2004).
- [46] D. R. Thompson, M. Lemere and Y. C. Tang, Nucl. Phys. **A286**, 53 (1977).